Atmospheric degradation correction of terahertz beams using multiscale signal restoration

Choonwoo Ryu* and Seong G. Kong

Department of Electrical and Computer Engineering, Temple University, Philadelphia, Pennsylvania 19122, USA

*Corresponding author: choonwoo@temple.edu

Received 28 October 2009; revised 11 January 2010; accepted 15 January 2010; posted 20 January 2010 (Doc. ID 119163); published 9 February 2010

We present atmospheric degradation correction of terahertz (THz) beams based on multiscale signal decomposition and a combination of a Wiener deconvolution filter and artificial neural networks. THz beams suffer from strong attenuation by water molecules in the air. The proposed signal restoration approach finds the filter coefficients from a pair of reference signals previously measured from low-humidity conditions and current background air signals. Experimental results with two material samples of different chemical compositions demonstrate that the multiscale signal restoration technique is effective in correcting atmospheric degradation compared to individual and non-multiscale approaches. © 2010 Optical Society of America

OCIS codes: 300.6495, 110.7410, 200.4260.

1. Introduction

Rapid progress in the development of the sources and detectors for generating and detecting the radiation in the terahertz (THz) frequency range realizes a wide variety of useful applications in spectroscopy [1–3], imaging [4,5], and communications [6,7]. THz spectroscopy has demonstrated a great potential to detect various chemical or biological agents through the identification of unique spectral absorption patterns of the material. Since THz beams can penetrate many nonmetallic materials, such as paper, textiles, and wood panels, THz spectroscopy can detect concealed threat materials from a distance. In addition, THz radiation does not cause harmful ionization effects, as do x-rays or gamma rays, because of its low photon energy, which presents an advantage of body safety in THz measurement settings. The THz range of the spectrum offers a broader communication bandwidth than the microwave range and enables secure, line-of-sight communication capabilities.

0003-6935/10/050927-09$15.00/0

THz beams are absorbed by molecules when they propagate through the atmosphere. THz spectroscopy and imaging with the power and efficiency of currently available radiation sources and detectors undergo technical challenges, such as strong attenuation in the atmosphere and spurious peaks in the spectra produced mainly by water vapor. These molecules create several absorption bands [8] or frequency bands of high attenuation. Such false peaks and dips make it difficult to identify material-specific signatures in the THz spectroscopic measurements. Atmospheric degradation of THz signals significantly reduces the signal-to-noise ratio in THz signal measurements and, therefore, limits the distance of signal sensing and transmission. THz signal restoration from atmospheric attenuation is important to increase the range of THz spectroscopic measurements and transmission, especially in humid atmospheric conditions.

Signal restoration can be defined as a deconvolution process to restore an original signal from the observed signal that is deformed by a degradation process and the noise [9]. The objective of THz signal restoration is to remove the effects of atmospheric attenuation from the THz signal observed in the open

air. Several approaches have been studied to restore THz signals from atmospheric attenuation. An adaptive deconvolution technique using prior knowledge of water absorption peaks is introduced by Withayachumnankul *et al.* [10] for removing the water vapor effects from observed THz signals. This approach utilizes the frequency and strength information of known water absorption peaks to find the best parameters for the modeled peaks that correspond to the measured absorption peaks. This approach has the advantage of adaptive removal of water absorption peaks without training measurements. However, only premodeled absorption peaks can be removed from the observed signal, not other unmodeled degradation effects. Furthermore, certain meaningful signatures from the THz measurement may be lost if the THz signal from a target sample has an overlapped frequency response with the modeled water vapor response, because the parameter tuning algorithm will be forced to match to the reference response by changing the model parameters. Similar approaches have been presented by Wang *et al.* [11,12]. These model-based approaches have an advantage of no training stage before the signal measurements, but are effective only for the premodeled frequency response of water vapor, not for unmodeled responses that need to be removed from the degradation. Polynomial modeling of the THz absorbance spectrum [13] approximately models the absorbance by a low-order polynomial from the observed measurements and finds matched absorbance from the prestored absorbance of contraband. This modeling may not be useful for general THz signal restoration. Our previous approach [14] utilizes an artificial neural network (ANN) to restore a THz signal from atmospheric degradation with no prior knowledge of degradation process models. The proposed multiscale signal restoration technique decomposes a THz signal into approximation and detail components using the discrete wavelet transform (DWT). A signal restoration filter consisting of a Wiener filter and an ANN removes atmospheric degradation for each individual component.

Wavelet analysis decomposes a signal into approximation and detail components in different scales using the contracted and dilated versions of a wavelet function [15]. The DWT has been widely used in signal processing applications. A combined use of the DWT and Wiener filtering was applied to signal denoising in multisensor signal estimation [16]. It has also been demonstrated that the learning performance of ANNs is improved by multiresolution signal decomposition [17,18]. Application examples of multiresolution decomposition in THz signal processing include denoising [2,19], THz image compression and classification [20], and multiscale image segmentation in THz computed tomographic imaging systems [21]. In [19], THz measurements with additive noise are used to compare denoising performances of different wavelets. A THz classification system utilizes wavelet denoising techniques for preprocessing of the THz signals [22]. These techniques focus on noise removal from THz signals by thresholding small wavelet coefficients, rather than a through a systematic approach to restoration of THz signals from atmospheric degradation.

This paper presents an atmospheric degradation correction technique of THz beams based on multiscale signal decomposition, which does not require the knowledge of the frequencies of absorption peaks to be removed. An observed THz signal is decomposed into approximation and detail components using the DWT. The restoration filter consists of a Wiener deconvolution filter and an ANN. For each component, a Wiener deconvolution filter is designed using the input–output signal, where the input is a degraded THz signal and the output is a desired signal obtained in low-humidity conditions. A Wiener deconvolution filter is an optimal filter that minimizes the error when the input signal contains noise. An ANN is trained for restoring the residual signal component that could not be restored in Wiener filtering. A combined Wiener filter and ANN, trained separately using the approximation and the detail components, restores each signal component from the fluctuations and the noise that cause absorption bands in the spectrum observed in humid air conditions. The experiments with two materials of different chemical compositions in a humid condition demonstrate that the proposed restoration technique can remove atmospheric degradation due to humid air conditions, while preserving the spectral signatures of the material.

2. Terahertz Spectroscopy

Our time-domain THz spectrometer consists of a femtosecond laser, a photoconductive THz wave emitter, and an electro-optic (EO) detector [23,24]. Figure 1 shows an optical layout of the spectrometer used in this experiment, adopted from the technique presented by Wu *et al.* [23]. The laser source is a compact mode-locked fiber laser (IMRA femtolite 780) that emits approximately 100 fs laser pulses with a center wavelength of 780 nm, a repetition rate of 48 MHz, and an average power of 30 mW. The THz emitter is a photoconductive switch fabricated on a low-temperature-grown GaAs chip, and modulated by the amplified reference signal of a lock-in amplifier. The modulation amplitude and frequency are typically 200 V and 9.5 kHz, respectively. The average power of our THz beam is estimated to be about a few microwatts. The THz pulses, generated by the emitter, are focused onto a sample by a pair of off-axis parabolic mirrors. The THz beams, transmitted through or reflected by the sample, are then sent to an EO detector by another pair of parabolic mirrors. The THz path length from the THz emitter to the ZnTe EO crystal is about 1 m. The EO detector consists of a ZnTe crystal, a quarter-wave plate, a Wollaston prism, and a pair of photodiodes [23]. The probe beam, aligned by a pellicle beam splitter, travels collinearly with the THz beam through the

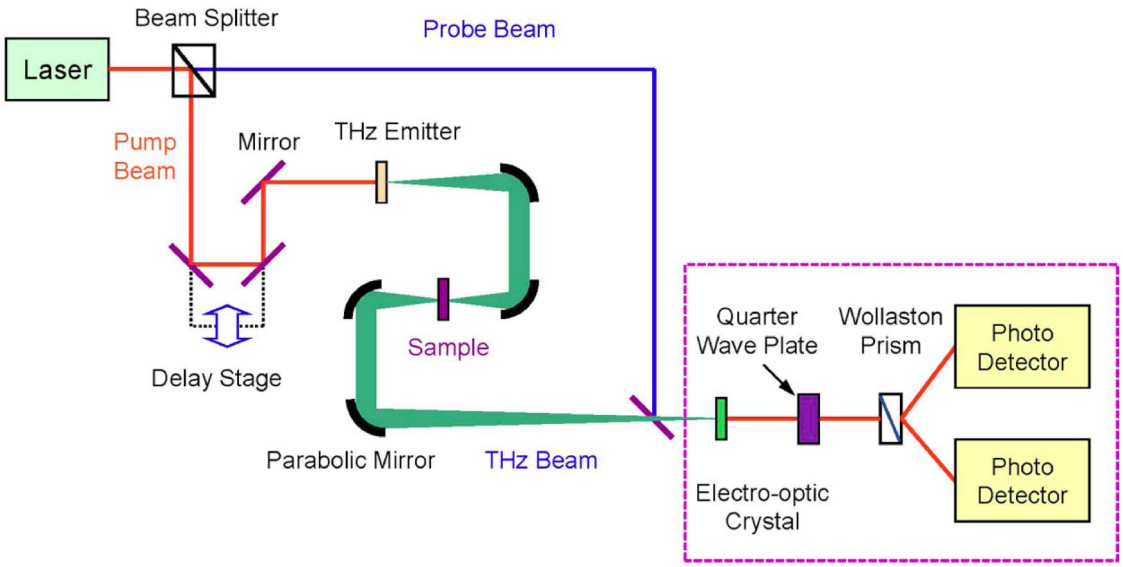

Fig. 1. (Color online) Schematic diagram of the time-domain terahertz spectrometer.

ZnTe EO crystal. Because of the EO effect of ZnTe crystal, the THz field results in a polarization change of the probe beam while it travels through the ZnTe crystal. The Wollaston prism separates the vertical-polarization and the horizontal-polarization components of the probe beam. These vertical and horizontal components are sent to the photodetector pair, which produces the differential photocurrents. Since the polarization of the probe beam is initially set to be 45°, the vertical and horizontal components are the same when the THz field is zero and, hence, there is no differential photocurrent. The difference between the electric currents and the photodiode pair is measured by a DSP lock-in amplifier (Stanford Research Systems SR-830) and a desktop computer.

3. Modeling of Terahertz Signal Degradation Process

A. Atmospheric Attenuation in the Terahertz Range

Atmospheric attenuation is the rate at which a beam's energy is absorbed via interactions with the atmosphere. Absorption is a main cause for the attenuation of a beam traveling through a medium. Absorption concerns the molecules gaining energy from the beam through collision. THz beams are absorbed by molecules when they propagate through the atmosphere. Nitrogen has no dipole moments and no energy transitions in the THz region. Hence, nitrogen will not be a major factor in the attenuation. Water vapor in the air generates absorption lines in the THz frequency range [1,2]. Water vapor is highly variable in the atmosphere, ranging from 0% to 0.4% of atmospheric content. Among the atmospheric constituents, water vapor is the largest contributor to atmospheric attenuation due to its variable content coupled with the strong interaction of water's electric dipole moment with electromagnetic radiation. With the power and efficiency of currently available THz radiation sources, strong absorption by water vapor in the atmosphere makes the range of THz sensing and transmission substantially short.

To show the atmospheric degradation effects, time-domain waveforms of THz signals are observed in

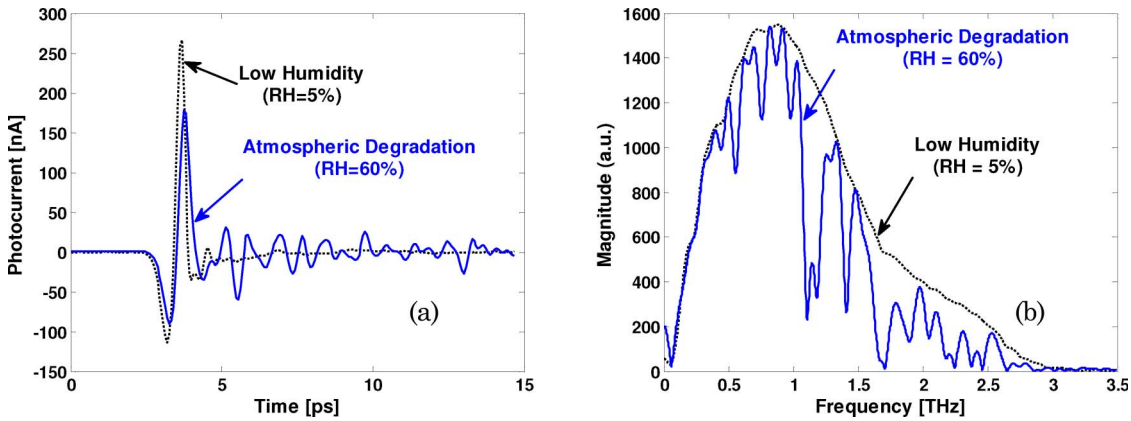

Fig. 2. (Color online) Atmospheric degradation of THz signals: (a) time waveforms, (b) Fourier spectra.

two humidity conditions: a low-humidity condition of less than 5% relative humidity (RH) and an open-air condition of 60% RH. The low-humidity condition is obtained by filling the measurement chamber of the THz spectrometer with dry nitrogen gas. Figure 2 compares time waveforms and Fourier spectra of THz signals measured at 18 °C in low humidity and in open air. The THz waveforms observed in a dry nitrogen gas condition show a smooth tail in approximately 5 ps and converge to zero current. However, the observed signals in open air show signal attenuation in the main peaks, with a slight time delay and strong fluctuations in the tail. In the Fourier spectrum domain, the THz signals observed in low-humidity conditions show a smooth spectrum over the THz range, while the signal in open air reveals several strong absorption bands.

B. Modeling of Atmospheric Degradation Process

A THz signal observed from a detector can be modeled as the output of an atmospheric degradation process with an additive external noise to an input signal generated from a THz source. The atmospheric degradation process is assumed as a system with characteristic function H. Then the THz signal degradation process can be expressed as

$$u(t) = H[r(t)] + v(t), \tag{1}$$

where $u(t)$ represents the observed degraded THz signal, $r(t)$ is the original undistorted signal from the THz source, and $v(t)$ denotes the additive external noise, which is assumed to be independent of $r(t)$. Figure 3 shows a general restoration process of THz signals from atmospheric degradation.

A signal restoration filter G takes the degraded signal $u(t)$ as an input and produces an output $x(t)$ that closely approximates the original signal $r(t)$:

$$x(t) = G[u(t)]. \tag{2}$$

If we assume that the inverse system of the degradation process H is known and well defined, the restored original signal $x(t)$ can be found by a direct inverse filtering:

$$x(t) = H^{-1}[u(t)]. \tag{3}$$

The objective of THz signal restoration is to find a restored signal $x(t)$ that is a faithful reproduction of the original signal $r(t)$ measured in low-humidity conditions. In this paper, the absorbance is utilized as a metric to determine if the restored signal $x(t)$ is sufficiently close to the reference signal $r(t)$ observed from a low-humidity condition. The absorbance of a signal $x(t)$ is with respect to a reference signal can be defined as

$$\text{Absorbance} = -\log_{10}\left(\frac{A^2_{\text{sample}}}{A^2_{\text{ref}}}\right), \tag{4}$$

where A_{sample} and A_{ref} indicate the magnitude Fourier spectra of the sample and the reference signal, respectively. Section 5 presents time waveforms and the absorption spectra, as well as relative improvement (RI), to provide visual and objective comparisons of the THz restoration techniques.

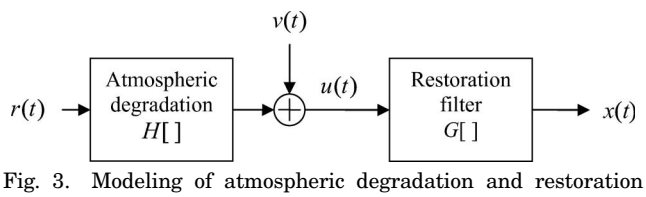

Fig. 3. Modeling of atmospheric degradation and restoration process of THz signals.

4. Atmospheric Degradation Restoration

A. Wavelet Analysis of Terahertz Signal

DWT decomposes a signal $x(t)$ into approximation and detail components by applying low-pass and high-pass filters to $x(t)$ [25]. The decomposed signals can be expressed as

$$A(t) = \sum_{k=-\infty}^{\infty} x(t)\varphi(t-k), \tag{5}$$

$$D(t) = \sum_{k=-\infty}^{\infty} x(t)\psi(t-k), \tag{6}$$

where approximation $A(t)$ and detail $D(t)$ components are generated by a low-pass filter $\varphi(t)$ and a high-pass filter $\psi(t)$. Figure 4 shows a level-2 wavelet decomposition of signal $x(t)$ using the DWT. The signals $A_1(t)$ and $D_1(t)$ represent level-1 approximation and detail components of signal $x(t)$. Level-1 approximation signal $A_1(t)$ is further decomposed into level-2 approximation and detail components.

Figure 5 shows the frequency response of level-2 decomposition results of a THz signal using the *symlet* wavelets, which are nearly symmetrical, modified from the Daubechies wavelets. The frequency range of interest is set to 0–3 THz because most frequency components of our THz measurements are contained in this range. The cutoff frequencies of neighboring filters are approximately 2 and 4 THz. Level-1 detail corresponds to a high-frequency range of over 4 THz, where no significant signal components exist and, therefore, the level-1 detail is removed for signal denoising. In the multiscale restoration method, level-2 approximation A_2 and detail D_2 are restored separately because they contain the characteristics of

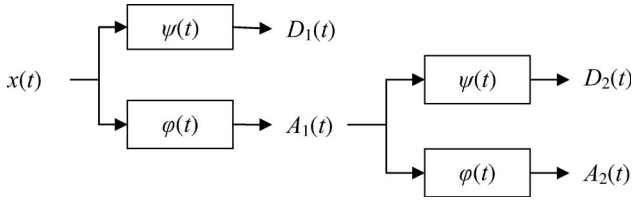

Fig. 4. Level-2 discrete wavelet decomposition of a signal.

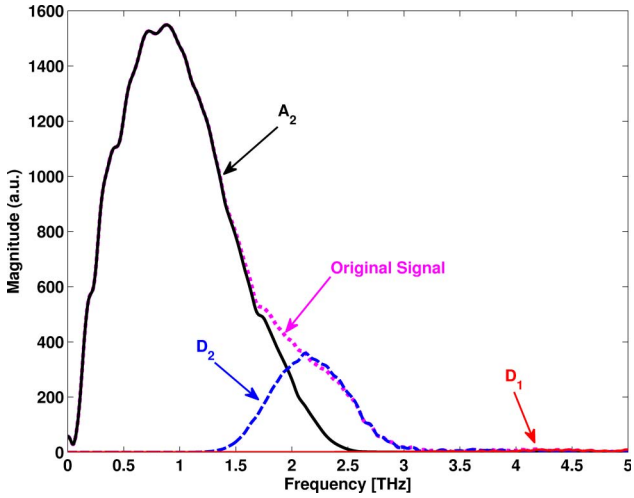

Fig. 5. (Color online) Fourier magnitude spectra of approximation and detail components in level-2 DWT decomposition.

the original signal in the ranges of 0–2 THz and 2–4 THz, respectively.

B. Atmospheric Degradation Restoration

The multiscale THz signal restoration technique uses a combined Wiener filter and ANN for each signal component. Figure 6 shows the idea of the proposed multiscale signal restoration technique. The observed THz signal $u(t)$ is decomposed in level 2 using the DWT for separate processing. The signals $g_A(t)$ and $g_D(t)$ denote approximation $A_2(t)$ and detail $D_2(t)$ components of level-2 wavelet decomposition. Each signal component is filtered by a combined Wiener deconvolution filter (W_A and W_D), and an ANN (N_A and N_D). The filters for the approximation component recover the signal in a frequency range of 0–2 THz and the filters for the detail component remove atmospheric degradation in a frequency range of 2–4 THz.

A degradation process at each decomposition level can be modeled by a linear system:

$$g_k(t) = h_k(t) * r_k(t) + v_k(t), \qquad k = A, D, \tag{7}$$

where $g_k(t)$ denotes DWT components of the observed THz signal $u(t)$, $h_k(t)$ is the impulse response of the atmospheric degradation process, $r_k(t)$ is the reference THz signal, and $v_k(t)$ is the additive noise. Wiener deconvolution filter $W(\omega)$ is used for restoration of the signal from overall atmospheric degradation:

$$W(\omega) = \frac{1}{H(\omega)} \frac{|H(\omega)|^2}{|H(\omega)|^2 + |V(\omega)|^2/|R(\omega)|^2}, \tag{8}$$

where $H(\omega)$ denotes the Fourier transform of the impulse response of the atmospheric degradation process $h(t)$, and $|V(\omega)|^2$ and $|R(\omega)|^2$ denote the power spectra of the noise $v(t)$ and the reference THz signal $r(t)$. The restored signal with a Wiener filter is given by

$$G'(\omega) = W(\omega)G(\omega), \tag{9}$$

where $G(\omega)$ and $G'(\omega)$ denote Fourier transforms of the degraded THz signal $g_k(t)$ and its Wiener restored signal $g'_k(t)$. Wiener deconvolution filters are determined using an input–output training dataset of the background air, where the input and the output are THz signals measured in low- and high-humidity conditions, respectively.

A nonlinear filter based on ANNs is used for the restoration of the residual signal that linear Wiener filtering is unable to recover. ANNs offer a model-free approach to the estimation of input–output characteristics of underlying nonlinear systems. Without a mathematical model of the restoration, a neural network adjusts its internal parameters using a representative set of training data. An ANN-based restoration filter $f(\,)$, trained using a set of input–output data pairs, finds a restored signal $c(t)$ from the output signal $g'(t)$ of the Wiener filter:

$$c(t) = f(\mathbf{g}'(t), \mathbf{s}). \tag{10}$$

Here $\mathbf{g}'(t)$ denotes an input vector of the signal generated by the Wiener filter and $\mathbf{s}$ indicates a parameter vector of its internal connection weights that need to be determined in the training process. A multilayer feed-forward neural network model [26] is used as an ANN-based restoration filter, with an input layer of $(2m+1)$ nodes and a single output node in the output layer. An input vector $\mathbf{g}'(t)$ consists of $(2m+1)$ delay-line elements of an input THz signal in a noncausal fashion:

$$\mathbf{g}'(t) = [g'(t - mI), \ldots, g'(t), \ldots, g'(t + mI)]^T, \tag{11}$$

where an integer I denotes the interval between adjacent data samples. The output of each layer is computed by a nonlinear activation function of a weighted sum of inputs from the previous layer. The neural network is trained using the backpropagation algorithm [27] to determine the internal parameter vector $\mathbf{s}$ from a set of training data pairs $(\mathbf{g}'_j, d_j)$, where d_j denotes the desired output for a given input $\mathbf{g}'_j$, i.e., the THz signal obtained in low-humidity conditions. In the multiscale restoration

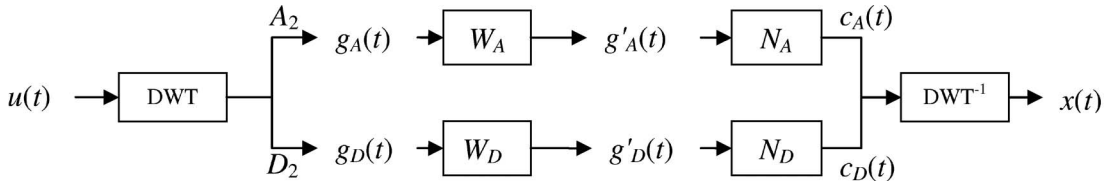

Fig. 6. Multiscale restoration filtering with Wiener filter and ANNs.

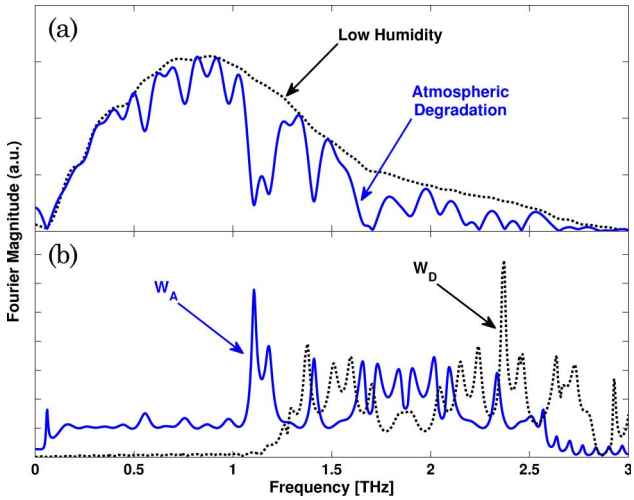

Fig. 7. (Color online) Frequency response of the Wiener deconvolution filters for approximation and detail components.

approach, two individual neural networks N_A and N_D are used for the restoration of residual signals of approximation and detail components.

5. Experiment Results

A time-domain THz spectrometer measured THz signals from different material samples. In this experiment, we used two solid substances with different chemical compositions, dinitrotoluene (DNT) and dinitrobutane (DNB). The testing samples were prepared in the form of a circular pellet of 25.4 mm diameter and thickness of 2.98 mm for DNT and 1.52 mm for DNB. The THz beam focused on the sample was approximately 2 mm in diameter. THz spectroscopic measurements were made in two different conditions: a low-humidity environment filled with dry nitrogen gas at less than 5% RH and an open-air environment at approximately 60% RH. From these measurements we obtained 42 datasets, of which we used 31 randomly selected datasets for training the signal restoration filters. The remaining 11 datasets were utilized for testing signal restoration performance.

In multiscale signal decomposition, the approximation component contains the overall shapes of the original signals and the detail includes high-frequency signal components. Figure 7 shows the frequency responses of the Wiener filters W_A and W_D for approximation and detail components. The locations of peaks of Wiener deconvolution filters W_A and W_D are observed to match with the major dips of the Fourier spectrum of degraded signals to recover atmospheric degradation. The filter response of W_D suppresses absorption in the 0–1.1 THz range, while the absorption dips over 2.5 THz range are corrected by filter W_D.

Figure 8 shows typical Fourier spectra of the materials DNT and DNB measured in low-humidity and open-air environments. The Fourier spectra show many spectral dips due to the absorption of water vapor in the THz range. Figure 9 demonstrates time-domain waveforms approximation and detail components generated by the multiscale restoration filter for DNT. In Fig. 9(a), the multiscale restoration filter restores the approximation component of the THz signal for DNT with high accuracy. For the detail component, strong fluctuations in the degraded signal are greatly removed, as shown in Fig. 9(b). The waveforms of the reference component and the detail component restored using the multiscale restoration technique overlap very closely. The restored detail component shows small errors in low-amplitude parts, where the estimation is difficult because the signal in this high-frequency range shows strong randomness. However, the error effect is minimal because the magnitude of the detail component is very small compared to approximation.

Figure 10 compares Fourier magnitude and absorption spectra of the multiscale restoration technique with the reference DNT signal. The Fourier magnitude spectrum of the restoration result is very close to that of the reference signal in the 0–3 THz range. All major dips in the frequency domain caused by atmospheric degradation shown in Fig. 8(a) are now successfully removed. The absorption spectrum of the restored signal is similar to the reference absorbance for the most part (0–2.3 THz), except where

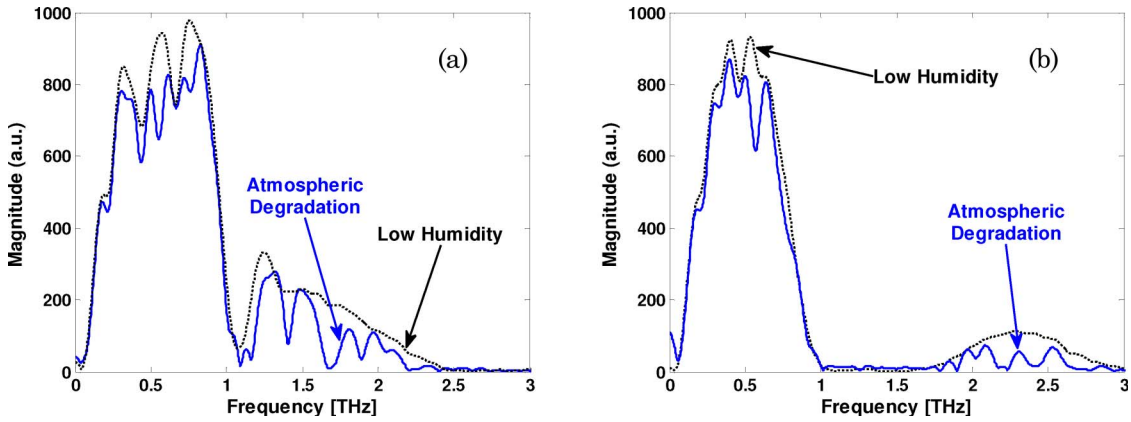

Fig. 8. (Color online) Fourier magnitude spectra of the testing samples: (a) DNT, (b) DNB.

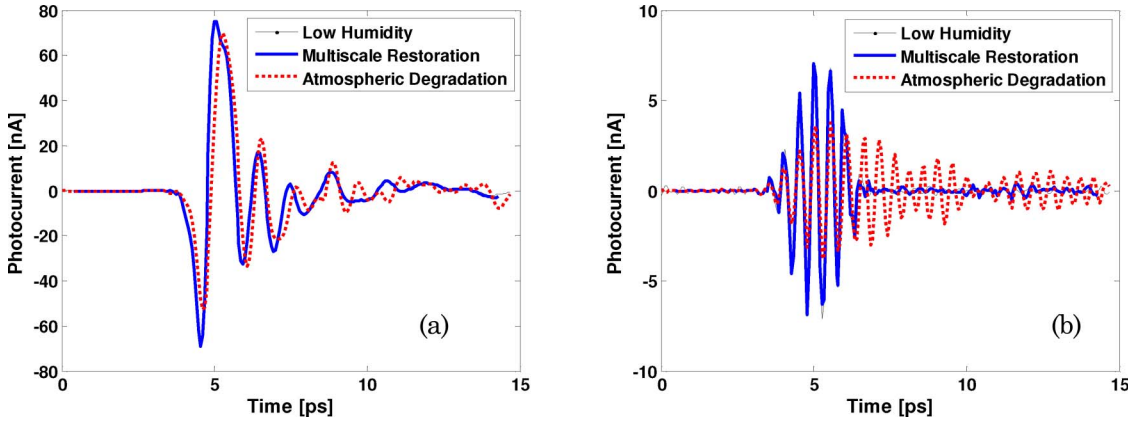

Fig. 9. (Color online) Time waveforms of the approximation and detail components restored using the multiscale restoration filter for DNT: (a) approximation (A_2), (b) detail (D_2).

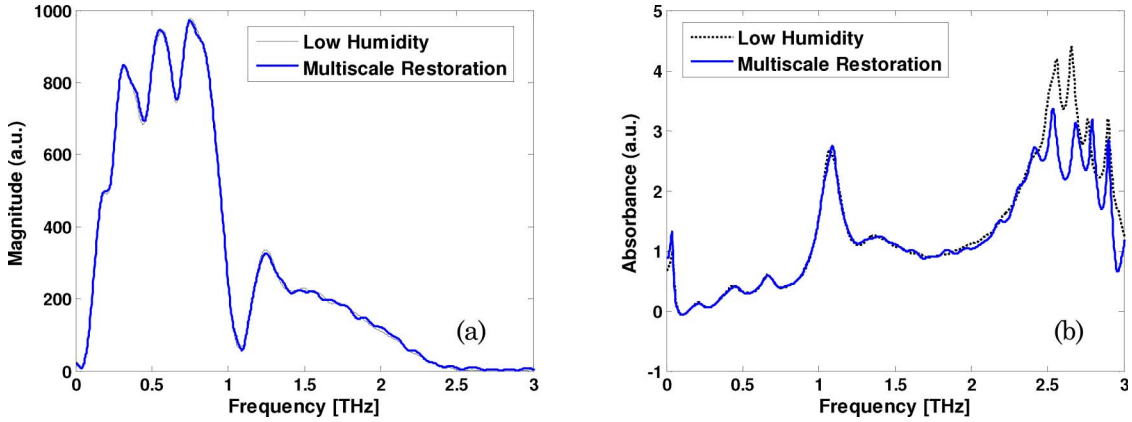

Fig. 10. (Color online) Fourier magnitude and absorption spectra of the multiscale restoration filter for DNT: (a) Fourier spectra, (b) absorbance.

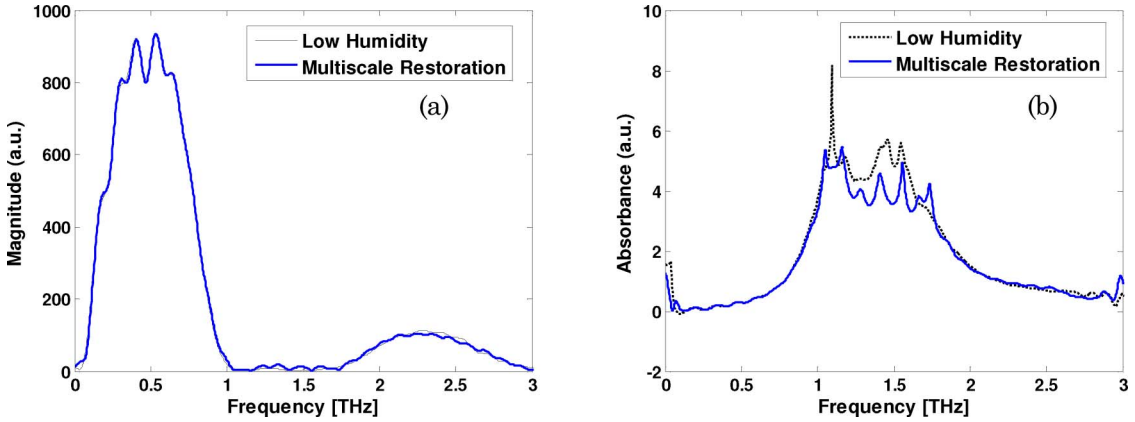

Fig. 11. (Color online) Fourier magnitude and absorption spectra of the multiscale restoration filter for DNB: (a) Fourier spectra, (b) absorbance.

Table 1. Comparison of Various Terahertz Signal Restoration Schemes in Relative Improvement

Materials	Wiener Only	ANN Only	Wiener + ANN	Multiscale Wiener + ANN
DNT	38.18	37.17	45.65	59.35
DNB	27.10	31.30	37.18	46.06

Fourier magnitude is very small and, therefore, the absorbance is sensitive to small changes even in low-humidity conditions. In Fig. 11, the multiscale restoration obtains similar results for the DNB sample. The restored Fourier spectrum is very close to that of the reference signal measured in a low-humidity condition. The reference spectrum of a DNB sample goes as low as the noise level in the 1–1.8 THz range, as shown in Fig. 11(a). Therefore, the absorbance, which is the ratio of spectral magnitudes of the restored and the reference signals, becomes very sensitive in this frequency range. Even though the restored spectral magnitude is very close to the reference spectrum, nonstationary absorbance peaks are observed in this range. We could observe a similar pattern for a DNT sample in the 2.5–3 THz range.

In order to compare different THz signal restoration methods using a metric that shows relative improvement (RI), the ratio of the mean-square errors of the restored signal and the reference signal is used in Table 1:

$$\mathrm{RI(dB)} = 10\log_{10}\left(\frac{\mathrm{MSE}_u}{\mathrm{MSE}_x}\right) = -10\log_{10}\left(\frac{\frac{1}{n}\sum \varepsilon_x^2(t)}{\frac{1}{n}\sum \varepsilon_u^2(t)}\right), \tag{12}$$

where $\varepsilon_x(t)$ denotes the error between restored signal $x(t)$ and the reference signal $r(t)$, $\varepsilon_x(t) = x(t) - r(t)$, and $\varepsilon_u(t)$ denotes the error between degraded signal $u(t)$ and the reference signal $r(t)$, $\varepsilon_u(t) = u(t) - r(t)$. Table 1 summarizes RI of various restoration schemes for the two chemical samples, Wiener filter only, ANN only, a combination of Wiener and ANN filters, and the multiscale restoration. For both chemicals, a combined Wiener and ANN filter shows some improvement over single-restoration-filter cases (Wiener only and ANN only). The multiscale Wiener and ANN restoration technique shows the biggest improvement of all combinations in THz signal restoration. The wavelet-based multiscale restoration method represents a THz signal with approximation and detail components that reveal low- and high-frequency characteristics of the signal. Wavelet transforms have a pyramidal tree structure, allowing successive decomposition of the lowest subband at each level, which means finer resolutions toward the lower frequency bands. In level-2 decomposition, the approximation component contains a low-frequency trend of a THz signal under 2.5 THz. The detail component (D_2) contains higher-frequency signal details for the range of approximately 1.3 to 3 THz, as shown in Fig. 5. A combined restoration filter designed for each individual component reduces the degradation effect separately.

6. Conclusion

Although THz radiation has demonstrated potential in detecting chemical substances from a distance, the sensing range is significantly limited due to strong attenuation by humid atmosphere. THz beams are absorbed by water molecules in the air when they propagate through the atmosphere. Therefore, it is difficult to obtain high signal-to-noise ratio with the power and efficiency of most currently available THz radiation sources and detectors. Material-specific THz signatures can be easily obscured by strong attenuation and spurious peaks in the absorption spectrum. This paper addresses a THz signal restoration technique to remove atmospheric degradation of a THz signal measured in the open air. THz signal restoration from atmospheric attenuation is important to increase the sensing range of THz signals in humid environments. The proposed approach is based on multiscale signal decomposition with combined signal restoration filters, a Wiener deconvolution filter and an ANN, for each signal component. A THz signal is decomposed into approximation and detail components using the DWT. A set of Wiener deconvolution filter and an ANN restore each signal component from the fluctuations and the noise that cause strong absorption bands in the spectrum. A restored THz signal is obtained by the inverse DWT of the filtered signal components. Experimental results with two chemical substances demonstrate that the multiscale signal restoration technique is effective in removing atmospheric degradation when compared to individual approaches.

References

1. M. v. Exter, C. Fattinger, and D. Grischkowsky, "Terahertz time-domain spectroscopy of water vapor," Opt. Lett. **14**, 1128–1130 (1989).
2. D. M. Mittleman, R. H. Jacobsen, R. Neelamani, R. G. Baraniuk, and M. C. Nuss, "Gas sensing using terahertz time-domain spectroscopy," Appl. Phys. B **67**, 379–390 (1998).
3. B. Ferguson and X.-C. Zhang, "Materials for terahertz science and technology," Nat. Mater. **1**, 26–33 (2002).
4. A. J. L. Adam, P. C. M. Planken, S. Meloni, and J. Dik, "Terahertz imaging of hidden paint layers on canvas," Opt. Express **17**, 3407–3416 (2009).
5. Y. C. Shen, T. Lo, P. F. Taday, B. E. Cole, W. R. Tribe, and M. C. Kemp, "Detection and identification of explosives using terahertz pulsed spectroscopic imaging," Appl. Phys. Lett. **86**, 241116 (2005).
6. R. Piesiewicz, T. Kleine-Ostmann, N. Krumbholz, D. Mittleman, M. Koch, J. Schoebel, and T. Kurner, "Short-range ultra-broadband terahertz communications: concepts and perspectives," IEEE Antennas Propagat. Mag. **49**, 24–39 (2007).
7. L. Möller, J. Federici, A. Sinyukov, C. Xie, H. C. Lim, and R. C. Giles, "Data encoding on terahertz signals for communication and sensing," Opt. Lett. **33**, 393–395 (2008).
8. H. M. Pickett, E. A. Cohen, B. J. Drouin, and J. C. Pearson, "Submillimeter, millimeter, and microwave spectral line catalog," Technical report (JPL, 2003).
9. R. W. Schafer, R. M. Mersereau, and M. A. Richards, "Constrained iterative restoration algorithm," Proc. IEEE **69**, 432–450 (1981).
10. W. Withayachumnankul, B. M. Fischer, and D. Abbott, "Numerical removal of water vapour effects from terahertz time-domain spectroscopy measurements," Proc. R. Soc. London Ser. A **464**, 2435–2456 (2008).
11. Y. Wang, Z. Zhao, Z. Chen, Y. Zhang, L. Zhang, and K. Kang, "Suppression of spectral interferences due to water-vapor rotational transitions in terahertz time-domain spectroscopy," Opt. Lett. **33**, 1354–1356 (2008).

12. Y. Wang, Z. Chen, Z. Zhao, L. Zhang, K. Kang, and Y. Zhang, "Restoration of terahertz signals distorted by atmospheric water vapor absorption," J. Appl. Phys. **105**, 103105 (2009).
13. Y. Wang, Z. Zhao, Z. Chen, K. Kang, B. Feng, and Y. Zhang, "Terahertz absorbance spectrum fitting method for quantitative detection of concealed contraband," J. Appl. Phys. **102**, 113108 (2007).
14. S. G. Kong and D. H. Wu, "Signal restoration from atmospheric degradation in terahertz spectroscopy," J. Appl. Phys. **103**, 113105 (2008).
15. M. Unser and T. Blu, "Wavelet theory demystified," IEEE Trans. Signal Process. **51**, 470–483 (2003).
16. A. M. Rao and D. L. Jones, "A denoising approach to multisensor signal estimation," IEEE Trans. Signal Process. **48**, 1225–1234 (2000).
17. Y. Liang and E. W. Page, "Multiresolution learning paradigm and signal prediction," IEEE Trans. Signal Process. **45**, 2858–2864 (1997).
18. Y. Liang and Xu Liang, "Improving signal prediction performance of neural networks through multiresolution learning approach," IEEE Trans. Syst. Man Cybern. B **36**, 341–352 (2006).
19. B. Ferguson and D. Abbott, "De-noising techniques for terahertz responses of biological samples," Microelectron. J. **32**, 943–953 (2001).
20. E. Berry, R. D. Boyle, A. J. Fitzgerald, and J. W. Handley, "Time-frequency analysis in terahertz-pulsed imaging," in *Computer Vision beyond the Visible Spectrum*, B. Bhanu and I. Pavlidis, eds. (Springer, 2005), pp. 276–311.
21. X. X. Yin, B. W.-H. Ng, B. Ferguson, S. P. Mickan, and D. Abbott, "Terahertz computed tomographic reconstruction and its wavelet-based segmentation by fusion," in *Proceedings of IEEE International Symposium on Industrial Electronics* (IEEE 2007), pp. 3409–3414.
22. X. X. Yin, B. W.-H. Ng, B. Ferguson, S. P. Mickan, and D. Abbott, "Statistical model for the classification of the wavelet transforms of T-ray pulses," in *Proceedings of International Conference on Pattern Recognition* (IEEE 2006), pp. 236–239.
23. Q. Wu, M. Litz, and X.-C. Zhang, "Broadband detection capability of ZnTe electro-optic field detectors," Appl. Phys. Lett. **68**, 2924–2926 (1996).
24. A. Garzarella, S. B. Qadri, T. J. Wieting, and D. H. Wu, "Spatial and temporal sensitivity variations in photorefractive electro-optic field sensors," Appl. Phys. Lett. **88**, 141106 (2006).
25. M. Vetterli and C. Herley, "Wavelets and filter banks: theory and design," IEEE Trans. Signal Process. **40**, 2207–2232 (1992).
26. S. W. Moon and S. G. Kong, "Block-based neural networks," IEEE Trans. Neural Netw. **12**, 307–317 (2001).
27. S. Haykin, *Neural Networks: A Comprehensive Foundation*, 2nd ed. (Prentice Hall, 1999).